

## Batteries

How to cite: *Angew. Chem. Int. Ed.* **2021**, *60*, 10871–10879

International Edition: doi.org/10.1002/anie.202101976

German Edition: doi.org/10.1002/ange.202101976

## Regulating the Solvation Sheath of Li Ions by Using Hydrogen Bonds for Highly Stable Lithium–Metal Anodes

Cheng Jiang<sup>†</sup>, Qingqing Jia<sup>†</sup>, Mi Tang, Kun Fan, Yuan Chen, Mingxuan Sun, Shuaifei Xu, Yanchao Wu, Chenyang Zhang, Jing Ma,<sup>\*</sup> Chengliang Wang,<sup>\*</sup> and Wenping Hu

**Abstract:** The performance of Li anodes is extremely affected by the solvation of Li ions, leading to preferential reduction of the solvation sheath and subsequent formation of fragile solid–electrolyte interphase (SEI), Li dendrites, and low coulombic efficiency (CE). Herein, we propose a novel strategy to regulate the solvation sheath, through the introduction of intermolecular hydrogen bonds with both the anions of Li salt and the solvent by small amount additives. The addition of such hydrogen bonds reduced the LUMO energy level of anions in electrolyte, promoted the formation of a robust SEI, reduced the amount of free solvent molecules, and enhanced stability of electrolytes. Based on this strategy, flat and dense lithium deposition was obtained. Even under lean electrolytes, at a current density of  $1 \text{ mA cm}^{-2}$  with a fixed capacity of  $3 \text{ mAh cm}^{-2}$ , the Li–Cu cells showed an impressive CE value of 99.2%. The Li–LiFePO<sub>4</sub> full cells showed long-term cycling stability for more than 1000 cycles at 1 C, with a total capacity loss of only  $15 \text{ mAh g}^{-1}$ .

## Introduction

The rising of energy demand is calling for alternatives of traditional lithium-ion batteries (LIBs).<sup>[1–10]</sup> In this regard, the lithium-metal batteries (LMBs) provide a new possibility for high energy density systems<sup>[8,11–18]</sup> by using Li metal as anodes, due to its ultrahigh theoretical capacity ( $3860 \text{ mAh g}^{-1}$ ) and low electrochemical potential ( $-3.04 \text{ V}$  vs. the standard hydrogen electrode). However, lithium metal is extremely

reactive with most organic electrolytes,<sup>[19,20]</sup> leading to low coulombic efficiency (CE).<sup>[21–28]</sup>

Even worse, it is well-known that lithium ions tend to form solvation sheath due to the interaction of Li ions with solvent molecules and anions.<sup>[29,30]</sup> The solvation sheath would diffuse together with the lithium ions and once touching the surface of lithium metal, it would be reduced firstly and turn into the main components of SEI,<sup>[31–34]</sup> which is fragile and inhomogeneous and will result in the propagation of lithium dendrites. Therefore, the solvation sheath plays an important role for the performance of LMBs.<sup>[35–37]</sup> In the solvation sheath, the anions are vital for the formation of high-quality SEI.<sup>[29,33,38,39]</sup> For example, due to the intensive ionic interaction<sup>[35,36,40]</sup> between Li<sup>+</sup> and NO<sub>3</sub><sup>-</sup>, the addition of LiNO<sub>3</sub> resulted in a solvation sheath with more NO<sub>3</sub><sup>-</sup> anions, leading to more favorable SEI with abundant LiN<sub>x</sub>O<sub>y</sub> species.<sup>[41]</sup> Besides LiNO<sub>3</sub>, the solvation sheath in high-concentration electrolyte<sup>[42–45]</sup> was of abundant anions of Li salt (i.e. TFSI<sup>-</sup>, FSI<sup>-</sup>), which could also promote a desirable highly-fluorinated SEI.<sup>[43,46–50]</sup> However, these achievements are either insufficient, or bearing the high cost and viscosity problems, which limits their practical applications.

Inspired by these pioneer works, herein, we proposed a novel strategy to regulate the solvation sheath of typical electrolyte systems, through introducing intermolecular hydrogen bonds by adding small amount additives (1,3,5-triformylphloroglucinol (TFP) was selected as a proof-of-concept, Figure 1a). To demonstrate the feasibility of this

[\*] C. Jiang,<sup>[†]</sup> Dr. M. Tang, Dr. K. Fan, Y. Chen, M. Sun, S. Xu, Y. Wu, C. Zhang, Prof. Dr. C. Wang  
School of Optical and Electronic Information, Wuhan National Laboratory for Optoelectronics (WNLO), Huazhong University of Science and Technology  
Wuhan 430074 (China)  
E-mail: clwang@hust.edu.cn

Q. Jia,<sup>[†]</sup> Prof. Dr. J. Ma  
School of Chemistry and Chemical Engineering, Nanjing University  
Nanjing 210093 (China)  
E-mail: majing@nju.edu.cn

Prof. Dr. W. Hu  
Tianjin Key Laboratory of Molecular Optoelectronic Sciences,  
Department of Chemistry, School of Sciences, Tianjin University  
Tianjin 300072 (China)

[†] These authors contributed equally to this work.

Supporting information and the ORCID identification number(s) for the author(s) of this article can be found under:  
https://doi.org/10.1002/anie.202101976.

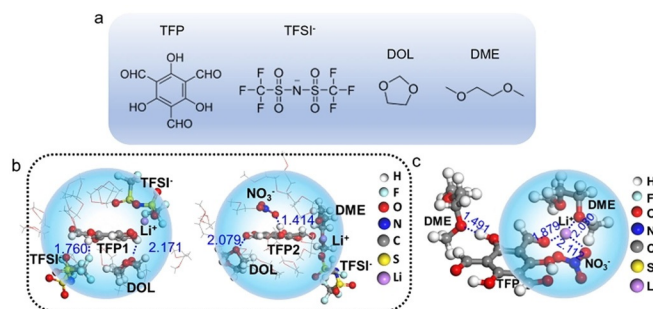


**Figure 1.** a) The chemical structures of TFP, ether solvents, and TFSI<sup>-</sup> anions. b) The selected MD snapshot at 4 ns with the highlight of the solvation sheath around two TFP molecules (TFP1 and TFP2), within 4 Å radius of the H atoms forming O–H bonds in TFP. c) The selected AIMD snapshot at 18 ps for illustration of the formation of hydrogen bonds. The interatomic distances are presented in the selected snapshots, in units of Å. The involved species are colored with Li = purple, N = blue, H = white, O = red, F = cyan, C = gray, and S = yellow.

strategy, the fluoride salts (LiTFSI and LiFSI, Figure 1 a) was adopted as the electrolyte, considering that the anions contain a lot of F atoms and the H...F bonds were the strongest hydrogen bonds. Simultaneously, ether-based solvent (Figure 1 a) was utilized to form H...O hydrogen bonds with the additives. In this case, the additives could form intermolecular hydrogen bonds with not only the anions but also the solvent molecules. Depending on the hydrogen bonds as well as the direct participation of TFP in the Li<sup>+</sup> solvation structure, the addition of TFP effectively regulated the solvation sheath. The presence of hydrogen bonds also reduced the LUMO (lowest occupied molecular orbital) energy levels of the anions and promoted the formation of desirable SEI with more LiF component. The resulted high-quality SEI led to homogeneous deposition of Li ions and effectively suppressed the formation of lithium dendrites.<sup>[35,51]</sup> Moreover, the introduction of hydrogen bonds also reduced the amount of free solvent molecules, leading to enhanced stability of the electrolytes. Consequently, the TFP assisted LMBs showed impressive CE and cycling stability even under lean electrolyte. Similar additives with weaker intermolecular hydrogen bonds were also studied as control experiments, showing the significance of intermolecular hydrogen bonds on the SEI formation and stable Li-metal anodes. These results shed light on a novel strategy to regulate the solvation sheath and pave a new way to construct reliable and high-performance LMBs.

## Results and Discussion

### Regulation of the Solvation Sheath

TFP was synthesized from phloroglucinol (PG) facilely and characterized according to literature<sup>[52]</sup> (Figure S1 and S2). To verify the introduction of intermolecular hydrogen bonds of the TFP additives with the anions (e.g. TFSI<sup>-</sup>, FSI<sup>-</sup>) of Li salt or the ether solvent, the nuclear magnetic resonance (NMR) spectra of different components were conducted. According to the <sup>1</sup>H NMR of TFP, the chemical shifts at around 14.14 and 10.18 could be assigned to the hydrogen atoms of -OH and -CHO groups in TFP, respectively (Figure 2 a).<sup>[53]</sup> The high chemical shifts should be ascribed to the intramolecular hydrogen bonds of TFP. With the addition of DME, the chemical shifts of -OH and -CHO groups showed an upfield displacement to 13.8 and 9.7, respectively. This displacement was most likely due to the addition of DME that could compete with the oxygen atoms in TFP to form intermolecular hydrogen bonds (-OH...O) with TFP and hence decreased the intramolecular hydrogen bonds in TFP. Subsequently, after adding LiTFSI, slight downfield shift of -OH can be observed, which can probably be ascribed to the formation of new hydrogen bonds of -OH...F. In the conjugated system of TFP, the -OH and -CHO were the electron donor and acceptor, respectively; and as a result, the -CHO showed similar change of downfield displacement with the -OH (Figure 2 a). The formation of -OH...F hydrogen bonds between TFP and TFSI<sup>-</sup> can be further confirmed by the upfield displacement of the chemical shift of TFSI<sup>-</sup> in the <sup>19</sup>F spectra (Figure 2 c).

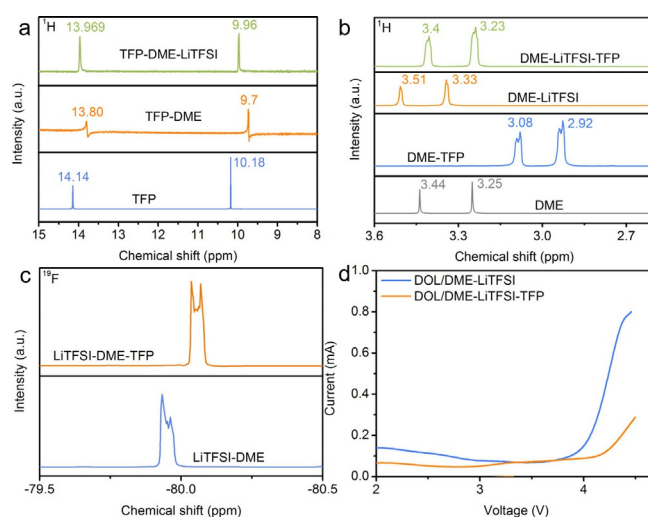


**Figure 2.** a) The <sup>1</sup>H NMR spectra of TFP in CHCl<sub>3</sub> without or with presence of DOL/DME or LiTFSI-DOL/DME (To monitor the real situation in the electrolyte, DOL/DME was added instead of DME. They have similar chemical environment of both H and O atoms). b) The <sup>1</sup>H NMR spectra of DME in CHCl<sub>3</sub> without or with presence of TFP, LiTFSI or LiTFSI-TFP. c) The <sup>19</sup>F NMR spectra of LiTFSI in CHCl<sub>3</sub> without or with presence of TFP (The electrolyte instead of LiTFSI was added into CHCl<sub>3</sub>, because the salt is not dissolved solely). d) The electrochemical stability of electrolyte (1 M LiTFSI in DOL/DME) with absence or presence of TFP.

In terms of the <sup>1</sup>H NMR spectra of DME, compared to the pure DME, the addition of Li<sup>+</sup> resulted in the downfield displacement of DME (Figure 2 b), which was likely due to the coordination of Li<sup>+</sup> with the oxygen atoms in DME and the electron-withdrawing property of Li<sup>+</sup>, leading to the deshielding effect on the hydrogen atoms of DME.<sup>[54,55]</sup> In the absence of Li<sup>+</sup>, after adding TFP into DME, although the formation of intermolecular hydrogen bonds between TFP and DME as mentioned above should also reduce the electrons on O<sub>DME</sub>, the whole electron-rich  $\pi$ -conjugated system of TFP probably brought the shielding effect on the hydrogen atoms of DME, leading to the upfield shift of DME (only introducing hydrogen bonds with absence of large conjugated system resulted in slight downfield shift of DME, as shown in Figure S3). However, when LiTFSI and TFP were both present, the chemical shifts of DME showed less variations, which should be ascribed to the stronger interactions between TFP and LiTFSI, reconfirming that TFP actually altered the structure of solvation sheath (including both solvent and anions).

Furthermore, the FTIR spectra (Figure S4) showed that after adding TFP into the electrolyte, the characteristic peak of C=O in -CHO groups of TFP shifted from 1665 cm<sup>-1</sup> (in pure TFP) to 1727 cm<sup>-1</sup> (in the electrolyte), which could be ascribed to the break of intermolecular hydrogen bonds between TFP molecules in the dilute solutions. On the other hand, the C-F peaks of LiTFSI at around 1062 cm<sup>-1</sup> in the DME-LiTFSI electrolytes shifted to 1057 cm<sup>-1</sup> and became broader after addition of TFP, which could be ascribed to the formation of hydrogen bonds between TFP with F atoms in TFSI<sup>-</sup>. Similarly, the C-O peaks of DME at around 1200 cm<sup>-1</sup>

in the DME-LiTFSI electrolytes also became broader after addition of TFP, indicating the formation of hydrogen bonds between TFP with O atoms in DME. These results agreed well with the NMR characterizations and indicated that the TFP could form intermolecular hydrogen bonds with the fluoride salts and the solvents and thereby regulate the solvation structure.

The possible formation of intermolecular hydrogen bonds between TFP and the anions (e.g., TFSI<sup>-</sup>) of Li salt or the ether solvents was demonstrated by using both force field-based molecular dynamics (MD) and *ab initio* molecular dynamics (AIMD), as shown in Figure 1b and Figure 1c, respectively. The simulation models used in MD and AIMD runs were listed in Table S1. To assess the role of TFP molecule that played in regulating the solvation sheath, we compared two different models: one consisted of 2TFP, 715DOL, 477DME, 39LiNO<sub>3</sub> and 100LiTFSI molecules to model the experimental conditions (1 M LiTFSI with 2 wt % LiNO<sub>3</sub> in 1:1 (v/v) DME and DOL, and 0.02 M TFP as additives), and the other model had the similar components but without TFP molecule (Table S1, Figure S5). The atomistic radial distribution functions (RDFs) between H atoms forming O–H bonds in TFP and hydrogen bond acceptors, such as O, N, F atoms from NO<sub>3</sub><sup>-</sup> and TFSI<sup>-</sup> ions as well as DME and DOL molecules were displayed in Figure S6a and S6e. The strong peaks at 1.5 Å (O–H...O, TFP/NO<sub>3</sub><sup>-</sup>) and 2.6 Å (O–H...N, TFP/NO<sub>3</sub><sup>-</sup>), respectively, indicated the formed hydrogen bond interactions between TFP and NO<sub>3</sub><sup>-</sup>. Although the peaks corresponding to TFP/DME&DOL and TFP/TFSI<sup>-</sup> were not as intensive as that of TFP/NO<sub>3</sub><sup>-</sup>, the peaks of 3.0 Å (O–H...O, TFP/TFSI<sup>-</sup>), 3.4 Å (O–H...N, TFP/TFSI<sup>-</sup>), 4.0 Å (O–H...F, TFP/TFSI<sup>-</sup>) and 4.7 Å (O–H...O, TFP/DME&DOL) could still be recognized easily (Figure S6b and S6f), indicating the possible formation of hydrogen bonds between TFP and the O, N and F atoms of TFSI<sup>-</sup> or the ether solvents. The hydrogen bonding interaction could be illustrated by the selected MD snapshot at 4 ns shown in Figure 1b, in which both of the two TFP molecules in our simulation models mentioned above showed short interactions with the salts and the solvents. Furthermore, AIMD simulations were carried out on the solvation shell of a TFP molecule within 5 Å radius (Figure 1c), which was taken from the selected 4 ns MD snapshot. The distance of O–H...O (MD: 1.41 Å; AIMD: 1.50–1.80 Å) formed between TFP and NO<sub>3</sub><sup>-</sup> was much less than the sum of the van der Waals atomic radius of O (1.52 Å) and H (1.20 Å), indicating the formation of O–H...O hydrogen bonds. Similarly, the distance of O–H...F (1.76 Å) was much less than the sum of the van der Waals atomic radius of F (1.47 Å) and H (1.20 Å), which indicated the formation of hydrogen bonds between TFP and TFSI<sup>-</sup>. The relatively weaker hydrogen bonding interactions were also observed between TFP and the O and N atoms of TFSI<sup>-</sup> or the ether solvents. MD simulations indicated that the TFP molecules could even directly participated in the solvation structure of Li ions, which could be confirmed by the analysis of RDFs between O atoms in TFP and Li<sup>+</sup> (showing obvious peak of Li–O at 2.0 Å) and the snapshots of the solvation sheath of Li<sup>+</sup> within 3 Å radius at 4 ns (showing TFP molecules in the solvation

structure of Li ions, Figure S5 and S6). It can be concluded from both MD and AIMD simulations that the addition of TFP could regulate the solvation structures through the interaction of intermolecular hydrogen bonds between the TFP molecules and the anions of Li salt (NO<sub>3</sub><sup>-</sup> and TFSI<sup>-</sup>) as well as the solvents (DME and DOL).

Consequently, as showed in Figure 2d, after adding TFP, the electrochemical stability of the electrolyte showed remarkable improvement. It has been reported that the cation-solvent complexes could lower the HOMO (highest occupied molecular orbital) energy levels of the solvent<sup>[46,56]</sup> and decrease the amount of free solvent molecules, leading to enhanced electrolyte stability. In this regard, the addition of TFP induced the intermolecular interaction with the TFSI<sup>-</sup> anions and therefore more DME/DOL molecules would coordinate with Li<sup>+</sup>, resulting in the decrease in free solvent molecules. The intermolecular interactions between TFP and the DME/DOL molecules could also reduce the free solvent molecules. The improved electrochemical stability reconfirmed that the presence of TFP altered the solvation sheath.

### The SEI Optimization

To evaluate the effect of the TFP and the regulation of solvation sheath on the formation of SEI, cyclic voltammetry (CV) test at voltage range of 0–2.5 V were performed. Compared with the CV curves of 1 M LiTFSI in DOL/DME, the addition of LiNO<sub>3</sub> (Figure 3a, the addition of LiNO<sub>3</sub> is also essential and the synergistic effect of LiNO<sub>3</sub> and TFP resulted in the high performance, see the following) showed a clear new reduction peak with onset potential of 1.7 V in the first cycle, which can be ascribed to the decomposition of LiNO<sub>3</sub>.<sup>[35]</sup> This can also be verified by the voltage plateau at around 1.5 V in the galvanostatic discharge curves (Figure S7). The small peak at around 1.06 V was likely corresponding to the decomposition of TFSI<sup>-</sup>.<sup>[35]</sup> The reduction peak lower than 0.5 V should be related to the underpotential deposition of Li.<sup>[57]</sup> As showed in Figure S7, the addition of TFP resulted in longer plateau at around 1.5 V, indicating that the addition of TFP also promoted the decomposition of LiNO<sub>3</sub>. More significantly, the addition of TFP led to much higher current peak at around 1.03 V (Figure 3b), indicating that the decomposition of TFSI<sup>-</sup> anions were promoted greatly in the initial cycle in the presence of TFP. Such phenomena could also be observed in the LiFSI-based electrolytes (Figure S8), which possessed similar structure to LiTFSI but showed intensive superiority in ionic conductivity, environmental benignity, and desirable SEI formation property.<sup>[42,58]</sup> The CV curves of LiFSI-based electrolytes also showed onset reduction potential at about 1.8 V, corresponding to the decomposition of LiNO<sub>3</sub>. Although the reduction potential of FSI<sup>-</sup> was overlapped with other reduction potentials and made it difficult to distinguish from them, the significant enhancement of the current intensity indicated the decomposition of FSI<sup>-</sup> at the similar voltage range.

The X-ray photoelectron spectroscopy (XPS) analysis of Cu electrode after one CV cycle was hence adopted to

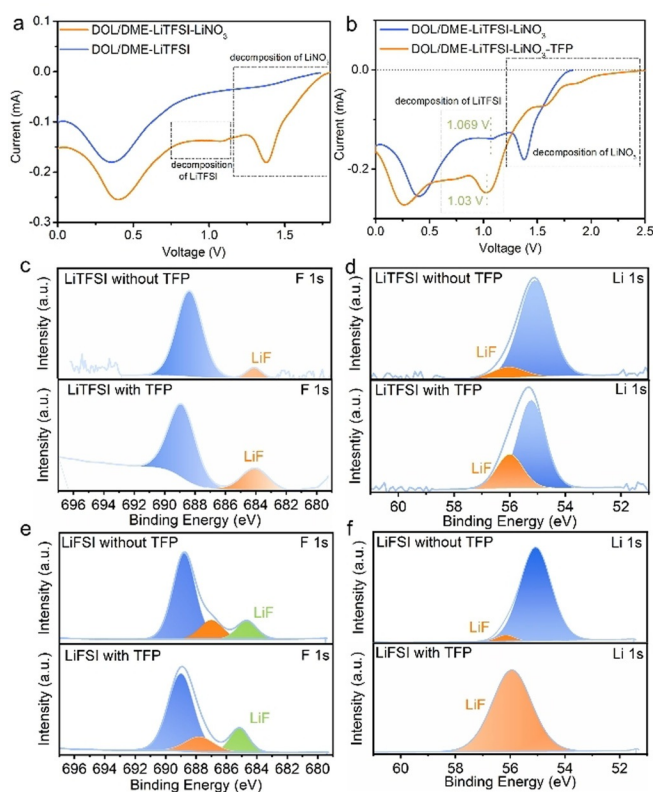


**Figure 3.** a,b) The CV curves of reduction behavior of different electrolytes. c–f) XPS characterization of SEI components formed on Cu electrode in different electrolytes after one cycle of CV test within 0–2.5 V: c) F 1s and d) Li 1s spectra of SEI in electrolyte (1 M LiTFSI in DOL/DME) with or without TFP, e) F 1s and f) Li 1s spectra of SEI in electrolyte (1 M LiFSI in DOL/DME) with or without TFP.

investigate the components of the formed SEI. As showed in the N 1s spectra (Figure S9), in the absence of TFP, obvious N content corresponding to  $\text{Li}_x\text{O}_y$ ,  $\text{NO}_2^-$  and  $\text{Li}_3\text{N}$  can be observed. However, after the addition of TFP, the relative intensity of  $\text{Li}_3\text{N}$  enhanced significantly, which could be ascribed to the more decomposition of LiTFSI (Figure S10). Similar results could be observed in the F 1s spectra (Figure 3c and e), in which the peaks at around 685 eV could be assigned to the LiF. Although the peak positions in LiTFSI (684.1 eV) and LiFSI ( $\approx 684.9$  eV) systems showed slight variations,<sup>[58,59]</sup> the LiF signals in both systems after adding TFP showed significantly higher intensity than that without TFP, indicating that the TFP indeed induced more LiF component in the SEI layer. Meanwhile, as showed in the Li 1s spectra (Figure 3d), compared to the weak LiF signal (56.5 eV) of the electrolyte without TFP, the addition of TFP resulted in obvious peak of LiF, which was consistent well with the F 1s spectra. Similar to the LiTFSI system, LiF took more dominant position in the SEI layer of the LiFSI based electrolytes with addition of TFP, which could be observed in the Li 1s spectra clearly (Figure 3e and f). Both the CV curves and the XPS results revealed that the addition of TFP facilitated the decomposition of anions of Li salts, and consequently, favorable SEI with abundant LiF composition was generated.

### The Growth Behavior of Li Deposition

As mentioned above, the improved SEI could be expected to provide homogeneous deposition of Li ions and suppress the formation of lithium dendrites effectively. Therefore, the scanning electron microscopy (SEM) was adopted to directly evaluate the morphology of deposited Li. At current density of  $1 \text{ mA cm}^{-2}$  and a deposited capacity of  $0.5 \text{ mAh cm}^{-2}$ , the high-quality SEI, which derived from TFP based electrolyte, led to reaction-controlled process of Li deposition.<sup>[50]</sup> As a result, the Li nuclei showed spherical morphology and compact stacking on the Cu substrate (Figure S11). However, the electrolytes without presence of TFP led to obvious dendritic morphology of deposited Li, and amounts of pits and dendrites can be observed, although there were still some spherical lithium nuclei. To further explore the self-amplification behavior of deposited Li, the SEM images of deposited Li with capacity of  $3 \text{ mAh cm}^{-2}$  were showed in Figure 4. In LiTFSI-based electrolytes without addition of TFP, the deposited Li showed large amounts of irregular pits and loose dendrites (Figure 4a and d). In sharp contrast, with the addition of TFP, the morphology of deposited Li was highly flat and dense (Figure 4b and e). In the LiFSI/TFP electrolytes, the deposited Li showed morphology without bulges and pits, and revealed extremely dense arrangement in large scale (Figure 4c and f). In addition, the Cu foils after deposition of Li in the LiFSI-based electrolytes with TFP were much more shining than that without TFP. The favorable morphology demonstrated that the presence of TFP could eliminate the formation and propagation of lithium dendrites effectively.

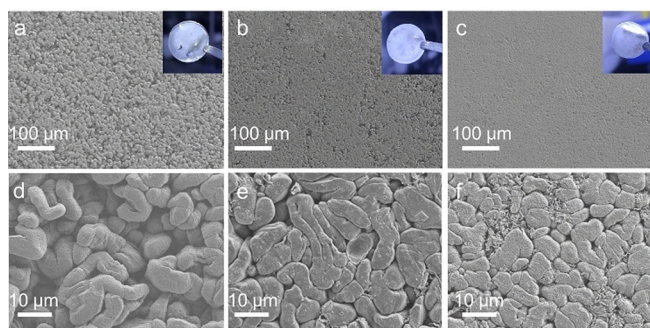


**Figure 4.** The morphology of deposited Li in a,d) LiTFSI based electrolytes without TFP, b,e) LiTFSI based electrolytes with TFP (0.02 M), c,f) LiFSI based electrolytes with TFP (0.02 M) with fixed capacity of  $3 \text{ mAh cm}^{-2}$ , at a current density of  $1 \text{ mA cm}^{-2}$ , (a)–(c) on a scale bar of  $100 \mu\text{m}$  and (d)–(f)  $10 \mu\text{m}$ . Inset of (a)–(c) showed the photo images of Cu foils after deposition of Li.

### Electrochemical Performance

Besides the visualized morphology illustrated in the SEM images, the electrochemical performance is also an important aspect to evaluate the regulated solvation sheath on the performance of Li metal anode. First of all, as showed in Figure 5a, the cyclic voltammety (CV) curves after introducing TFP additives showed higher overpotential and lower

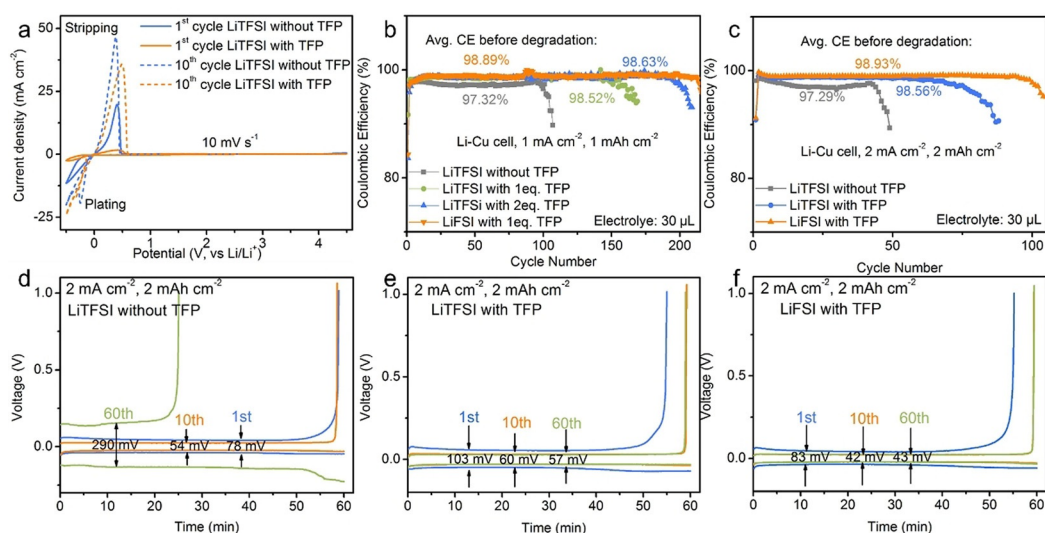


**Figure 5.** a) CV curves of Li-SS half cells in LiTFSI-based electrolyte with and without TFP (0.02 M). The CE of Li-Cu half cells in different electrolytes at b) current density of 1 mA cm<sup>-2</sup> with a fixed capacity of 1 mAh cm<sup>-2</sup> (1 equiv. = 0.02 M) and c) current density of 2 mA cm<sup>-2</sup> with a fixed capacity of 2 mAh cm<sup>-2</sup> (the concentration of TFP was 0.02 M). The voltage profiles of the 1st, 10th, and 60th cycle of LiTFSI-based electrolyte d) without and e) with TFP, and f) LiFSI-based electrolyte with TFP (the concentration of TFP was 0.02 M).

current in the first plating process. These results indicated that the addition of TFP induced slower initial electrochemical kinetics, probably due to the formation of SEI layer in the first cycle. However, after 10 cycles, the current peak of plating process in TFP-based electrolyte was higher than that without TFP, suggesting that the formed robust SEI layer with abundant LiF in the TFP-based electrolytes enhanced the conversion reaction between Li<sup>+</sup> and Li. Subsequently, the different electrolytes were applied in Li-Cu half cells to evaluate the effect of TFP.<sup>[38]</sup> In the Li-Cu cells, if the Li foil was used directly, the TFP would inevitably react with Li metal, leading to uncertain changes on the concentration of TFP, and the decreasing amount of TFP in the electrolyte only provided limited improvement to the performance of Li-Cu cells (Figure S12). In this regard, to avoid the direct reaction between Li foils and TFP, the Li foils were pre-modified by TFP (rinsing polished Li foils in the DME/TFP solution) before assembled in Li-Cu cells for those TFP were added. All the batteries were first cycled between 0 and 1 V at 50  $\mu$ A for 10 cycles to form a stable SEI on the electrodes. It was worth noting that in the TFP based electrolyte, the absence of LiNO<sub>3</sub> led to the coulombic efficiency (CE) even tend to be 0 (Figure S13); however, the coexistence of LiNO<sub>3</sub> and TFP resulted in a CE approaching 99% (Figure 5b), indicating that the SEI layer derived by LiNO<sub>3</sub> played an indispensable role in preventing the direct reaction between TFP and deposited lithium during the deposition process. What's more, at a current density of 1 mA cm<sup>-2</sup> with a fixed capacity of 1 mAh cm<sup>-2</sup>, the LiTFSI-based electrolyte without addition of TFP showed an average CE of 97.32% before degradation (excluding the 1st cycle). In sharp contrast, after addition of TFP (0.02 M), impressive improvement of CE and cycling stability can be obtained. The LiTFSI-based electrolyte with addition of TFP showed an average CE of 98.52% and improved cycling stability (from 100 cycles to more than 150 cycles). Even more, the LiFSI-based electrolyte with

addition of TFP showed an average CE of 98.89% and impressive cycling stability for more than 200 cycles. These results indicated that the synergistic effect of LiNO<sub>3</sub> and TFP determined the high performance. Besides, to evaluate how the amount of TFP affects the cycling performance of Li-Cu cells, the LiTFSI-based electrolyte with "2 equiv." TFP (i.e. 0.04 M) was adopted. With the increasing concentration of TFP, the cycling stability was prolonged (from 150 to 180 cycles) and the CE was enhanced to 98.63%, which demonstrated that it was possible to further improve the performance of Li-Cu cells through controlling the concentration of TFP (nevertheless, the concentration of TFP elsewhere was kept as 0.02 M, if without special note). On the other hand, when the concentration of TFP was increased to 0.1 M, although the average CE showed further enhancement (98.73%), the stability was decreased to around 120 cycles (Figure S14). The faded cycling stability may be ascribed to the overconsumption of the Li salts in the dilute electrolyte. When the capacity was increased to 3 mAh cm<sup>-2</sup>, the LiTFSI and LiFSI-based electrolytes with addition of TFP even showed remarkable CE of 99.1% and 99.2%, respectively (Figure S15). Furthermore, when the Li-Cu cell was tested at current density of 2 mA cm<sup>-2</sup> with a capacity of 2 mAh cm<sup>-2</sup>. The LiTFSI-based electrolyte without TFP showed an average CE only 97.29% and dropped quickly within 50 cycles (Figure 5c). However, the addition of TFP (0.02 M) promoted the CE impressively to 98.56%. The LiFSI-based electrolyte with addition of TFP even showed average CE of 98.93%. In addition, the charge and discharge curves revealed that although the initial voltage hysteresis (103 mV and 83 mV for LiTFSI and LiFSI-based electrolytes, respectively) of TFP based electrolytes were higher than that without TFP (78 mV, in LiTFSI-based electrolyte), the voltage hysteresis decreased quickly in the subsequent cycling (Figure 5d and f). The changes on voltage hysteresis were coincident with the CV curves as discussed above, indicating

that the formed robust SEI layer in the first cycle by the addition of TFP facilitated the reaction kinetics afterwards (Figure 5 a).

To further investigate the feasibility of TFP based electrolytes in more rigorous conditions, the current density was increased to  $5 \text{ mA cm}^{-2}$ , and the fixed capacity kept as  $1 \text{ mAh cm}^{-2}$ . As showed in Figure S16, with TFP, the Li-Cu cells showed higher CE and longer cycling stability than those without TFP. The LiFSI-based electrolyte still showed impressive cycling stability about 140 cycles, and an average CE of 97.9% could be obtained.

Besides, it was worth mentioning that the initial CE of TFP based electrolyte was always lower than that without TFP. It was likely due to the gradual formation of robust SEI layer in the first cycle and the inevitable reaction between Li and TFP in the initial cycle; however, the formed SEI would prevent the further side reactions and resulted in higher CE and longer cycle stability afterwards. Moreover, it indicated that besides the formed SEI components generated from the Li salts (LiTFSI,  $\text{LiNO}_3$ ), the products derived by direct reaction of TFP with Li would also have influences on the SEI. To evaluate the function of products derived from Li and TFP in LMBs, Li foil was first modified by TFP, and then the Li-Cu half cells was assembled without addition of TFP in the electrolytes. As showed in Figure S17, the as-prepared Li-Cu cells still showed improvement of CE and cycling stability compared to those without pre-modification of Li foils in the same electrolyte, indicating that the organic components derived from the reaction of Li and TFP also had positive influences on forming high-quality SEI.

We also assembled Li-Li cells to further confirm the impressive cycling performance in TFP based electrolytes. The long-term cycling stability of Li-Li cells at a current

density of  $3 \text{ mA cm}^{-2}$  with a capacity of  $1 \text{ mAh cm}^{-2}$  were showed in Figure S18. Without addition of TFP, the Li-Li cells showed higher overpotential, and after 100 h, sudden voltage drop can be observed, indicating the internal short circuit. But the cells with TFP-based electrolyte showed lower overpotential and a long-term cycling stability for more than 1000 h.

### Electrochemical Performance of Li-LFP Full Battery

In order to investigate the feasibility of TFP-based electrolyte in practical LMBs,  $\text{LiFePO}_4$  (LFP) cathode was utilized to pair with either excessive or limited Li in full cells. Here, LiTFSI DOL/DME system was chosen instead of LiFSI DOL/DME, due to the wider electrochemical window than that of LiFSI system (Figure S19 and S20). In the LiTFSI-based electrolyte without addition of TFP, the capacity of Li-LFP full cells showed continuous decay and the CE showed obvious fluctuation during cycling (Figure 6 a, b and c), which should be ascribed to the consumption of electrolyte and internal short circuit due to the growth of Li dendrites. However, the presence of TFP enhanced the stability of Li-LFP full cells impressively. Capacity loss of only  $15 \text{ mAh g}^{-1}$  was obtained after 1000 cycles. What is more, the average CE was more than 99.8% within 1000 cycles.

For the practical application of LMBs, the N/P ratio should be as low as possible. In this regard, limited Li was adopted as the anode ( $2.6 \text{ mAh}$ ,  $\text{Capacity}_{\text{Li}}/\text{Capacity}_{\text{LFP}} = 1$ ) to explore the performance of Li-LFP full cells under the same conditions. The limited Li anode was prepared through pre-deposition of Li on Cu substrate in the electrolytes (with or without TFP) same with the related full cells. At a current

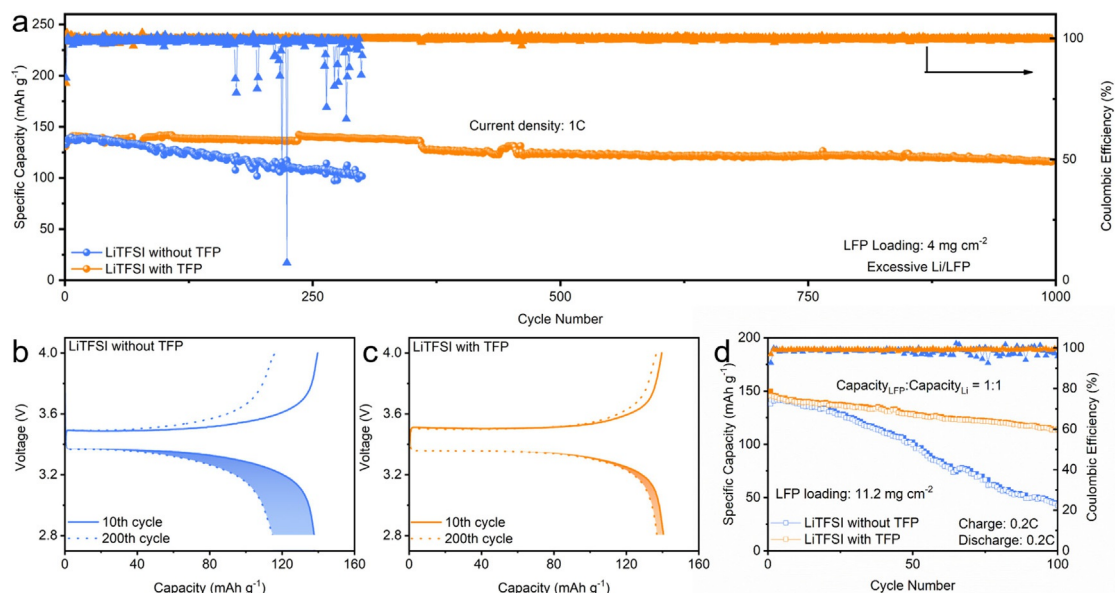


**Figure 6.** a) Cycling performance of Li-LFP full cells with excessive Li as the anodes in the LiTFSI-based electrolytes with or without addition of TFP (0.02 M) at a current density of 1 C. Corresponding voltage profiles of Li-LFP full cells after 10 cycle and 200 cycles in electrolyte b) without TFP and c) with TFP. d) Cycling performance of Li-LFP full cells with limited Li as anodes in the LiTFSI-based electrolytes with or without addition of TFP (0.02 M), at current density of 0.2 C. The amount of the electrodes was set under condition of  $\text{Capacity}_{\text{anode}}/\text{Capacity}_{\text{cathode}} = 1$ .

density of 0.2 C, the Li-LFP full cells in electrolyte without TFP showed obvious capacity loss and fluctuation of CE after 20 cycles. However, in TFP based electrolyte, the capacity retention and CE of Li-LFP full cell showed obvious superiority, indicating lower Li consumption rate during the cycling (Figure 6d).

### Similar Additives with Weaker Intermolecular Hydrogen Bonds

All of these results indicated that the TFP could effectively regulate the solvation sheath, promote the decomposition of anions in the initial cycle and generate robust SEI with abundant LiF and  $\text{LiN}_x\text{O}_y$  by forming hydrogen bond with solvent and anions. The enhanced SEI enabled the Li dendrite-free and high-CE LMBs. These results encouraged us to further manipulate the hydrogen bonds for tuning the electrochemical performance, by adjusting the chemical structures of the additives. It is well known that the formyl group (-CHO) in TFP is electron-withdrawing group, and hence it will facilitate the dissociation of hydroxyl group (-OH) and the subsequent formation of strong hydrogen bonds with the solvent molecules and anions in the electrolyte. Therefore, similar structures with less formyl groups (e.g. 2,4,6-trihydroxybenzaldehyde (THB)) or without formyl groups (phloroglucinol (PG)) were tested. It could be inferred that THB should produce weaker hydrogen bonds with the solvent molecules and anions; while PG would lead to the weakest hydrogen bonds. As showed in Figure S21a, the Li-Cu cells tested in electrolytes with PG cannot be operated normally. It indicated that the products derived from Li and PG were of high resistance, which can be proved by the electrochemical impedance spectroscopy (Figure S21b). On the contrary, in the electrolytes with THB, the Li-Cu cell showed moderately improved cycling stability and average CE of 98.13% (Figure S22). Nevertheless, the CE was still lower than that with addition of TFP. These results indicated that the -CHO played an essential role for forming hydrogen bonds with the solvent molecules and anions, and the subsequent regulation of SEI layers.

Density functional theory (DFT) was further performed to analyze how the additives influence the LUMO energy levels of the anions and solvents. TFP and PG were selected as the proof of concept. As showed in Figure 7 and Table S2, the LUMO energy level of LiTFSI was  $-1.40$  eV; however, after the formation of TFP-LiTFSI complex, the LUMO of the complex reduced by 0.95 and 1.01 eV, respectively, for the two different configurations of the complex. The reduction of LUMO energy levels should be the reason that TFP facilitated the decomposition of LiTFSI as mentioned above. On the contrary, for the complex of PG-LiTFSI, the LUMO energy levels were even elevated. The elevated LUMO energy levels should be the reason that the presence of PG would rather suppress the decomposition of anions. These theoretical calculations were consistent well with the behavior of SEI formation in TFP or PG-based electrolyte, as showed in Figure S23. Besides, in the LiFSI system, after the formation of PG-LiFSI and TFP-LiFSI complexes, the LUMO energy levels showed similar changes to those in the

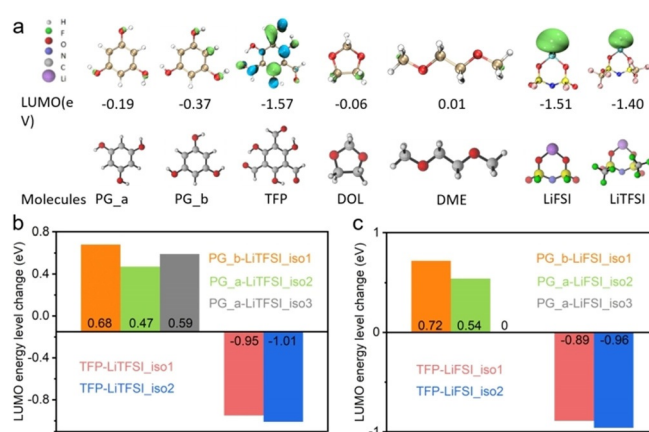


**Figure 7.** a) The chemical structures and LUMO energy levels of PG, TFP, DOL, DME, LiFSI and LiTFSI. PG\_a and PG\_b represent the two conformations of PG. b) The LUMO energy level changes of LiTFSI after the formation of PG-LiTFSI and TFP-LiTFSI complexes. c) The LUMO energy level changes of LiFSI after the formation of PG-LiFSI and TFP-LiFSI complexes. Iso- represents the different isomers.

LiTFSI system. The DFT calculation concluded that the TFP could realize the effective regulation of solvation sheath and optimization of SEI by forming hydrogen bonds through -OH groups with F atoms in the TFSI<sup>-</sup> or FSI<sup>-</sup> anions and O atoms in ether solvents, which were facilitated by the -CHO groups. Further improvements would be achieved by subtle controlling the polar functional groups (e.g. -OH, -SH, NH etc.) as well as the structures (e.g. conjugated systems, electron-withdrawing groups) linked to these functional groups for effectively manipulating the hydrogen bonds and the subsequent solvation structures. However, it also should be noted that too active functional groups or materials (e.g. water or acid) would definitely do harm to the Li anodes and are not suitable for this strategy.

### Conclusion

In summary, we proposed a novel strategy to regulate the solvation sheath and SEI, through introducing intermolecular hydrogen bonds by adding small amount additives, which is able to construct dendrite-free and high-CE LMBs. Depending on the hydrogen bond with solvent and anions, the TFP additive can effectively stabilize the solvents and promote the formation of robust SEI with abundant LiF and  $\text{LiN}_x\text{O}_y$ . The resulted favorable SEI led to impressive enhancement of CE in the Li-Cu half cells under lean electrolyte of 30  $\mu\text{L}$ . Considerable CE of 99.2% could be obtained at a current density 1  $\text{mA cm}^{-2}$  with a fixed capacity of 3  $\text{mAh cm}^{-2}$ . The TFP assisted Li-LFP full cells showed long-term cycling stability for more than 1000 cycles and the average CE was more than 99.8%. Similar additives with weaker intermolecular hydrogen bonds were also studied as control experiments, showing the significance of intermolecular hydrogen bonds on the SEI formation and stable Li-metal anodes. The altered behavior of anions and solvents was further validated by the DFT calculations. This work shed light on a new

mechanism for regulating solvation sheath and constructing high-quality SEI, and provided a new choice of the functional additives for reliable LMBs.

### Acknowledgements

This work was financially supported by the National Natural Science Foundation of China (51773071, 21873045, 22033004), the National 1000-Talents Program, the Innovation Fund of WNLO, the Fundamental Research Funds for the Central Universities (HUST: 2018KFYXKJC018 and 2019kfyRCPY099), the Open Fund of the State Key Laboratory of Integrated Optoelectronics (IOSKL2020KF02) and China Postdoctoral Science Foundation (2020M672323). The authors thank the HUST Analytical & Testing Center for characterizations.

### Conflict of interest

The authors declare no conflict of interest.

**Keywords:** electrolyte additives · hydrogen bonds · lithium anodes · solid–electrolyte interphase · solvation chemistry

- [1] M. Armand, J.-M. Tarascon, *Nature* **2008**, *451*, 652–657.
- [2] M. Tang, S. Zhu, Z. Liu, C. Jiang, Y. Wu, H. Li, B. Wang, E. Wang, J. Ma, C. Wang, *Chem* **2018**, *4*, 2600–2614.
- [3] Y. Chen, C. Wang, *Acc. Chem. Res.* **2020**, *53*, 2636–2647.
- [4] M. Tang, C. Jiang, S. Liu, X. Li, Y. Chen, Y. Wu, J. Ma, C. Wang, *Energy Storage Mater.* **2020**, *27*, 35–42.
- [5] Y. Chen, M. Tang, Y. Wu, X. Su, X. Li, S. Xu, S. Zhuo, J. Ma, D. Yuan, C. Wang, W. Hu, *Angew. Chem. Int. Ed.* **2019**, *58*, 14731–14739; *Angew. Chem.* **2019**, *131*, 14873–14881.
- [6] C. Jiang, M. Tang, S. Zhu, J. Zhang, Y. Wu, Y. Chen, C. Xia, C. Wang, W. Hu, *Angew. Chem. Int. Ed.* **2018**, *57*, 16072–16076; *Angew. Chem.* **2018**, *130*, 16304–16308.
- [7] H. Dai, K. Xi, X. Liu, C. Lai, S. Zhang, *J. Am. Chem. Soc.* **2018**, *140*, 17515–17521.
- [8] D. Lin, Y. Liu, Y. Cui, *Nat. Nanotechnol.* **2017**, *12*, 194–206.
- [9] Y. Zhu, J. Li, X. Yun, G. Zhao, P. Ge, G. Zou, Y. Liu, H. Hou, X. Ji, *Nano Micro Lett.* **2020**, *12*, 12–16.
- [10] W. Hong, A. Wang, L. Li, T. Qiu, J. Li, Y. Jiang, G. Zou, H. Peng, H. Hou, X. Ji, *Adv. Funct. Mater.* **2020**, *30*, 2000756.
- [11] Y. Guo, H. Li, T. Zhai, *Adv. Mater.* **2017**, *29*, 1700007.
- [12] Y. Zhang, T.-T. Zuo, J. Popovic, K. Lim, Y.-X. Yin, J. Maier, Y.-G. Guo, *Mater. Today* **2020**, *33*, 56–74.
- [13] Y. Liu, X. Yin, X. Shen, P. Zou, X. Qin, C. Yang, Q. Zhang, F. Kang, G. Chen, B. Li, *Adv. Funct. Mater.* **2020**, *30*, 2002522.
- [14] J. Alvarado, M. A. Schroeder, T. P. Pollard, X. Wang, J. Z. Lee, M. Zhang, T. Wynn, M. Ding, O. Borodin, Y. S. Meng, K. Xu, *Energy Environ. Sci.* **2019**, *12*, 780–794.
- [15] H. Li, D. Chao, B. Chen, X. Chen, C. Chuah, Y. Tang, Y. Jiao, M. Jaroniec, S. Z. Qiao, *J. Am. Chem. Soc.* **2020**, *142*, 2012–2022.
- [16] W. Zhou, S. Wang, Y. Li, S. Xin, A. Manthiram, J. B. Goodenough, *J. Am. Chem. Soc.* **2016**, *138*, 9385–9388.
- [17] S. Bai, Y. Sun, J. Yi, Y. He, Y. Qiao, H. Zhou, *Joule* **2018**, *2*, 2117–2132.
- [18] S. H. Wang, Y. X. Yin, T. T. Zuo, W. Dong, J. Y. Li, J. L. Shi, C. H. Zhang, N. W. Li, C. J. Li, Y. G. Guo, *Adv. Mater.* **2017**, *29*, 1703729.
- [19] J. B. Goodenough, Y. Kim, *Chem. Mater.* **2010**, *22*, 587–603.
- [20] W. Xu, J. Wang, F. Ding, X. Chen, E. Nasybulin, Y. Zhang, J.-G. Zhang, *Energy Environ. Sci.* **2014**, *7*, 513–537.
- [21] J. Xiang, L. Yang, L. Yuan, K. Yuan, Y. Zhang, Y. Huang, J. Lin, F. Pan, Y. Huang, *Joule* **2019**, *3*, 2334–2363.
- [22] X. Zhang, A. Wang, X. Liu, J. Luo, *Acc. Chem. Res.* **2019**, *52*, 3223–3232.
- [23] J. Chazalviel, *Phys. Rev. A* **1990**, *42*, 7355–7367.
- [24] X. Shen, H. Ji, J. Liu, J. Zhou, C. Yan, T. Qian, *Energy Storage Mater.* **2020**, *24*, 426–431.
- [25] K. Yan, J. Wang, S. Zhao, D. Zhou, B. Sun, Y. Cui, G. Wang, *Angew. Chem. Int. Ed.* **2019**, *58*, 11364–11368; *Angew. Chem.* **2019**, *131*, 11486–11490.
- [26] H. Shi, J. Qin, K. Huang, P. Lu, C. Zhang, Y. Dong, M. Ye, Z. Liu, Z. S. Wu, *Angew. Chem. Int. Ed.* **2020**, *59*, 12147–12153; *Angew. Chem.* **2020**, *132*, 12245–12251.
- [27] D. H. Liu, Z. Bai, M. Li, A. Yu, D. Luo, W. Liu, L. Yang, J. Lu, K. Amine, Z. Chen, *Chem. Soc. Rev.* **2020**, *49*, 5407–5445.
- [28] S. Li, Z. Luo, L. Li, J. Hu, G. Zou, H. Hou, X. Ji, *Energy Storage Mater.* **2020**, *32*, 306–319.
- [29] Y. Jie, X. Liu, Z. Lei, S. Wang, Y. Chen, F. Huang, R. Cao, G. Zhang, S. Jiao, *Angew. Chem. Int. Ed.* **2020**, *59*, 3505–3510; *Angew. Chem.* **2020**, *132*, 3533–3538.
- [30] X. Chen, X. Shen, B. Li, H. J. Peng, X. B. Cheng, B. Q. Li, X. Q. Zhang, J. Q. Huang, Q. Zhang, *Angew. Chem. Int. Ed.* **2018**, *57*, 734–737; *Angew. Chem.* **2018**, *130*, 742–745.
- [31] W. Zhao, L. Zou, J. Zheng, H. Jia, J. Song, M. H. Engelhard, C. Wang, W. Xu, Y. Yang, J. G. Zhang, *ChemSusChem* **2018**, *11*, 2211–2220.
- [32] H. Ye, Y.-X. Yin, S.-F. Zhang, Y. Shi, L. Liu, X.-X. Zeng, R. Wen, Y.-G. Guo, L.-J. Wan, *Nano Energy* **2017**, *36*, 411–417.
- [33] M. D. Tikekar, S. Choudhury, Z. Tu, L. A. Archer, *Nat. Energy* **2016**, *1*, 16114.
- [34] Y. Lu, M. Tikekar, R. Mohanty, K. Hendrickson, L. Ma, L. A. Archer, *Adv. Energy Mater.* **2015**, *5*, 1402073.
- [35] X.-Q. Zhang, X. Chen, L.-P. Hou, B.-Q. Li, X.-B. Cheng, J.-Q. Huang, Q. Zhang, *ACS Energy Lett.* **2019**, *4*, 411–416.
- [36] C. Yan, H. R. Li, X. Chen, X. Q. Zhang, X. B. Cheng, R. Xu, J. Q. Huang, Q. Zhang, *J. Am. Chem. Soc.* **2019**, *141*, 9422–9429.
- [37] X. Chen, Q. Zhang, *Acc. Chem. Res.* **2020**, *53*, 1992–2002.
- [38] B. D. Adams, J. Zheng, X. Ren, W. Xu, J.-G. Zhang, *Adv. Energy Mater.* **2018**, *8*, 1702097.
- [39] Z. Yu, D. G. Mackanic, W. Michaels, M. Lee, A. Pei, D. Feng, Q. Zhang, Y. Tsao, C. V. Amanchukwu, X. Yan, H. Wang, S. Chen, K. Liu, J. Kang, J. Qin, Y. Cui, Z. Bao, *Joule* **2019**, *3*, 2761–2776.
- [40] X. Q. Zhang, X. Chen, X. B. Cheng, B. Q. Li, X. Shen, C. Yan, J. Q. Huang, Q. Zhang, *Angew. Chem. Int. Ed.* **2018**, *57*, 5301–5305; *Angew. Chem.* **2018**, *130*, 5399–5403.
- [41] S. S. Zhang, *J. Electrochem. Soc.* **2012**, *159*, A920–A923.
- [42] J. Qian, W. A. Henderson, W. Xu, P. Bhattacharya, M. Engelhard, O. Borodin, J.-G. Zhang, *Nat. Commun.* **2015**, *6*, 6362.
- [43] X. Ren, L. Zou, X. Cao, M. H. Engelhard, W. Liu, S. D. Burton, H. Lee, C. Niu, B. E. Matthews, Z. Zhu, C. Wang, B. W. Arey, J. Xiao, J. Liu, J.-G. Zhang, W. Xu, *Joule* **2019**, *3*, 1662–1676.
- [44] J. Zheng, G. Ji, X. Fan, J. Chen, Q. Li, H. Wang, Y. Yang, K. C. DeMella, S. R. Raghavan, C. Wang, *Adv. Energy Mater.* **2019**, *9*, 1803774.
- [45] L. Yu, S. Chen, H. Lee, L. Zhang, M. H. Engelhard, Q. Li, S. Jiao, J. Liu, W. Xu, J.-G. Zhang, *ACS Energy Lett.* **2018**, *3*, 2059–2067.
- [46] X. Ren, L. Zou, S. Jiao, D. Mei, M. H. Engelhard, Q. Li, H. Lee, C. Niu, B. D. Adams, C. Wang, J. Liu, J.-G. Zhang, W. Xu, *ACS Energy Lett.* **2019**, *4*, 896–902.
- [47] L. Suo, O. Borodin, T. Gao, M. Olguin, J. Ho, X. Fan, C. Luo, C. Wang, K. Xu, *Science* **2015**, *350*, 938.
- [48] C. Jiang, Y. Gu, M. Tang, Y. Chen, Y. Wu, J. Ma, C. Wang, W. Hu, *ACS Appl. Mater. Interfaces* **2020**, *12*, 10461–10470.

- [49] X. Fan, L. Chen, X. Ji, T. Deng, S. Hou, J. Chen, J. Zheng, F. Wang, J. Jiang, K. Xu, C. Wang, *Chem* **2018**, *4*, 174–185.
- [50] X. R. Chen, Y. X. Yao, C. Yan, R. Zhang, X. B. Cheng, Q. Zhang, *Angew. Chem. Int. Ed.* **2020**, *59*, 7743–7747; *Angew. Chem.* **2020**, *132*, 7817–7821.
- [51] X.-Q. Zhang, X.-B. Cheng, X. Chen, C. Yan, Q. Zhang, *Adv. Funct. Mater.* **2017**, *27*, 1605989.
- [52] J. H. Chong, M. Sauer, B. O. Patrick, M. J. MacLachlan, *Org. Lett.* **2003**, *5*, 3823.
- [53] H. Li, M. Tang, Y. Wu, Y. Chen, S. Zhu, B. Wang, C. Jiang, E. Wang, C. Wang, *J. Phys. Chem. Lett.* **2018**, *9*, 3205–3211.
- [54] X. Bogle, R. Vazquez, S. Greenbaum, A. Cresce, K. Xu, *J. Phys. Chem. Lett.* **2013**, *4*, 1664–1668.
- [55] W. Zhang, Q. Wu, J. Huang, L. Fan, Z. Shen, Y. He, Q. Feng, G. Zhu, Y. Lu, *Adv. Mater.* **2020**, *32*, 2001740.
- [56] X. Chen, H. R. Li, X. Shen, Q. Zhang, *Angew. Chem. Int. Ed.* **2018**, *57*, 16643–16647; *Angew. Chem.* **2018**, *130*, 16885–16889.
- [57] C. Yan, Y. X. Yao, X. Chen, X. B. Cheng, X. Q. Zhang, J. Q. Huang, Q. Zhang, *Angew. Chem. Int. Ed.* **2018**, *57*, 14055–14059; *Angew. Chem.* **2018**, *130*, 14251–14255.
- [58] M. Wang, L. Huai, G. Hu, S. Yang, F. Ren, S. Wang, Z. Zhang, Z. Chen, Z. Peng, C. Shen, D. Wang, *J. Phys. Chem. C* **2018**, *122*, 9825–9834.
- [59] Y. Han, Y. Jie, F. Huang, Y. Chen, Z. Lei, G. Zhang, X. Ren, L. Qin, R. Cao, S. Jiao, *Adv. Funct. Mater.* **2019**, *29*, 1904629.

Manuscript received: February 8, 2021

Accepted manuscript online: February 25, 2021

Version of record online: April 6, 2021